Inorganic Chemistry

Article

pubs.acs.org/IC

Rhodium Amidinate Dimers as Structural and Functional Hubs for Multimetallic Assemblies

Daniel Chartrand and Garry S. Hanan*

Department of Chemistry, Université de Montréal, Montréal, Quebec, H3T 1J4 Canada

Supporting Information

ABSTRACT: The synthesis and characterization of multichromophore assemblies based on a dirhodium tetra-*N,N′*-diphenylisonicotinamidinate dimer are reported. The pyridyl moieties were used to coordinate up to four positively charged rhenium(I) chromophores of the form *fac*-[Re(bpy)(CO)$_3$**L**]PF$_6$ (bpy = 2,2′-bipyridine, **L** = a pyridyl group on the Rh$_2$ dimer). The mono-, bis-, tris-, and tetrarhenium assemblies were isolated by size-exclusion chromatography, and their spectroscopic and electrochemical properties were studied and compared with DFT and time-dependent (TD) DFT models of the original rhodium dimer and the mono- and tetrarhenium assembly. The rhenium chromophores modify the properties of the rhodium dimer: for example, the first oxidation of the Rh$_2$ dimer (Rh−Rh δ^* orbital) increased from the original 210 mV versus SCE in acetonitrile, by 45 mV per rhenium complex added, finishing at 390 mV for the tetrarhenium complex. The rhodium dimers display solvatochromism with acetonitrile (MeCN) due to the formation of an axial adduct and has an association constant that increased by a factor of 3.8 when the dimer has four rhenium chromophores. The absorption data clearly exhibited the cumulative effect of the addition of rhenium chromophores in the 230 to 400 nm range. The main visible band, a metal-dimer-to-ligand charge transfer (^{1}M$_2$LCT) transition determined by TD-DFT, red-shifts from 541 nm to 603 nm, while the main near-IR band, a ^{1}Rh$_2$($\pi^*\rightarrow\sigma^*$) transition, has a small blue-shift (∼26 cm^{-1}/Re), varying from 837 to 831 nm upon addition of the four Re(I) chromophores. This was observed in TD-DFT also with a total shift of 105 cm^{-1} for the tetrarhenium assembly. In terms of emission, the rhenium excited state was completely quenched upon coordination to the dimer, suggesting fast electron transfer of the rhodium dimer. All other aspects of the rhenium chromophore are similar to the parent complex where **L** = pyridine, showing similar redox couples and additive spectral characteristics.

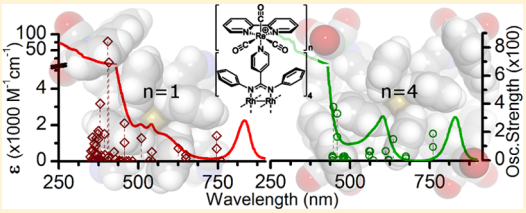

INTRODUCTION

The rhodium dimer with its paddle-wheel motif is greatly affected by the nature of its four ligands.[1] Its tetra-acetate and tetracarboxamidinate form are effective catalysts,[2] its bis-acetate form has anticancer properties,[3] and in general it serves as a building block for supramolecular assemblies.[4] Amidinate-based rhodium dimers have a chemistry of their own and have been studied for the last 30 years.[5] They are in general more inert then their acetate analogues, but still possess rich electrochemistry and photochemistry, making them an interesting choice from which to build polynuclear complexes.[6]

Rhenium triscarbonyl diimine chromophores also possess a very rich history due to their high stability, high-energy excited state, and capacity for reductive and oxidative quenching of their excited state.[7] They can also be functionalized to form supramolecular assemblies.[6a,b] As such, they are good candidates for functional assemblies, since they can act as photosensitizers that supply electrons for catalysts (e.g., hydrogen evolution),[8] as photocatalysts that reduce carbon dioxide to carbon monoxide,[9] or as photosensitizers for other processes, such as photoisomerization.[10] The rhenium archetype used in this study is [Re(bpy)(CO)$_3$L]$^+$, where bpy = 2,2′-bipyridine and L is a neutral ligand.

In natural photosynthetic systems, light energy is gathered by light-harvesting antennae and is subsequently transferred to a reaction center.[11] Our approach to gather light energy involves attaching chromophores to the paddle-wheel motif of the rhodium dimer, thus grafting up to four chromophores in a very close space with a strict 90° angle between each metal center, similar to tetrapyridylporphyrin assemblies.[12] Both tetra-amidinate and tetra-acetate rhodium dimers have been designed to incorporate functional groups able to bond to metal ions.[6a,b,13] The tetra-amidinate dimers were found to be more robust and allowed subsequent reactions to be performed on the metal dimer.[6a] We have already demonstrated the use of isonicotinic amidinate rhodium dimers to assemble four rhenium chromophores, but since the dimer themselves are not known as active catalysts, unsaturated assemblies (one to three chromophores) are more promising, as they intrinsically possess further coordination sites to make larger assemblies of chromophores or even complete photocatalytic systems. The properties of these four units, **1** to **4** as seen in Chart 1 (full in Chart S1), are presented herein, with a focus on the effect on the dimer core upon addition of each rhenium chromophore and the coordination of axial acetonitrile. To this end, theoretical calculations were also performed to establish and

Received: November 4, 2013
Published: December 17, 2013

dx.doi.org/10.1021/ic4024585 | *Inorg. Chem.* 2014, 53, 624−636

Chart 1. Rh_2 Complexes 1 to 5 Synthesized in This Study and Side-View with an MeCN Adduct

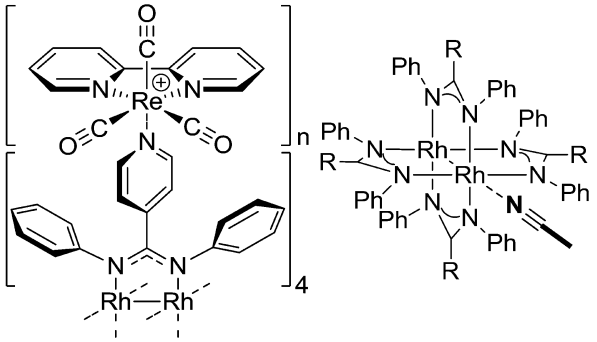

1, n = 1; **2**, n = 2; **3**, n = 3; **4**, n=4; **5**, n = 0.

correlate the structural and functional properties of the assemblies.

EXPERIMENTAL SECTION

General Considerations. The organic reagents were obtained from Sigma Aldrich, rhenium carbonyl and rhodium(II) acetate from Pressure Chemical Co., and solvents from Fischer and Anachemia. All were used as received. IR spectra were recorded on solid samples using a diamond ATR Perkin-Elmer Spectrum 100 FT-IR. Nuclear magnetic resonance spectra were recorded using Bruker spectrometers (300, 400, and 700 MHz) at room temperature, with ^1H and ^{13}C chemical shifts referenced to residual solvent resonances (1.94 and 1.24 ppm, respectively, for CD_3CN). Elemental analyses were performed on the desolvated bulk samples by the university departmental service. All photophysical measurements were done in air-equilibrated solvents, using a borosilicate cell. Absorption and emission spectra were recorded at room temperature using a Cary 500i UV−vis−NIR spectrophotometer and a Cary Eclipse 300 fluorimeter, respectively. Association constants were measured by titration of acetonitrile and were calculated using multiple wavelengths with the HypSpec software suite.[14] The emission spectra used the maximum of absorption of the lowest energy band of the sample as excitation wavelength. Electrochemical measurements were carried out in argon-purged solvent at room temperature with a BAS CV50W multipurpose apparatus. The working electrode was a Pt electrode, the counter electrode was a Pt wire, and the pseudoreference electrode was a silver wire. The reference was set using an internal 1.0 mM ferrocene sample with its redox couple adjusted to 400 mV versus SCE in acetonitrile and 460 mV versus SCE in dichloromethane.[15] The concentration of the compounds was about 1.0 mM, tetrabutylammonium hexafluorophosphate (TBAP) was used as supporting electrolyte, and its concentration was 0.10 M. Cyclic voltammograms were obtained at scan rates of 10, 100, and 200 mV/s. For reversible processes, half-wave potentials (vs SCE) were measured as the average potential of the anodic and cathodic peak and compared with square wave voltammetry (SWV) experiments performed with a step rate of 4 mV, a square wave amplitude of 25 mV, and a frequency of 15 Hz. For irreversible oxidation processes, the cathodic peak was used as E_p and the anodic peak was used for irreversible reduction processes. The criteria for reversibility were the separation of 60 mV between cathodic and anodic peaks, the close to unity ratio of the intensities of the cathodic and anodic currents, and the constancy of the peak potential on changing scan rate. Experimental uncertainties are as follows: absorption maxima, ±2 nm; molar absorption coefficient, 10%; emission maxima, ±5 nm; redox potentials, ±10 mV.

Synthetic Methods. The rhenium complexes $Re(CO)_5Br$,[16] *fac*-$[Re(bpy)(CO)_3Br]$,[17] *fac*-$[Re(bpy)(CO)_3(CH_3CN)][PF_6]$,[18] *fac*-$[Re(bpy)(CO)_3(pyridine)][PF_6]$[18] (**8**), and *fac*-$[Re(bpy)(CO)_3(THF)][PF_6]$[19] were prepared as described. The syntheses of the tetra(*N,N′*-diphenylisonicotinamidinate)dirhodium(II) dimer (**5**) and the tetra-$[Re(bpy)(CO)_3]-[Rh_2(dppy)_4]$ tetrahexafluorophosphate (**4**) were previously published by our group, with a more complete characterization given herein.[6b] See Figure 5 (top) for the labeling of the proton peaks in NMR.

General conditions for the synthesis of **1**, **2**, **3**, and **4**: To a 50 mL round-bottomed flask were added **5** (0.312 g, 0.241 mmol) and $[Re(bpy)(CO)_3(NCCH_3)]PF_6$ (0.470 g (0.767 mmol) in acetone (20 mL). The solution was heated at reflux and was monitored by TLC. After 2 h, reaction equilibrium was reached (TLC R_f (7 CH_3CN:1 KNO_3(aq) (v/v)): 0.75 (**5**); 0.70 (**1**); 0.68 (**2**); 0.62 (**3**); 0.60 (**4**)). The solution was evaporated to dryness at room temperature and purified by multiple size-exclusion chromatography columns (Sephadex-LH20 gel; column: 3 cm diameter by 1.2 m length; solvent: 0.45 acetonitrile/0.45 methanol/0.1 water (v/v/v)), flow rate: 30 mL per hour, total elution time to first fraction: 16 h). The fractions were treated with dilute aqueous KPF_6 (5% of volume); then the solvent was reduced until precipitation of a green solid, which was filtered and washed with water and then dried under vacuum. Alternate synthesis: Using $[Re(bpy)(CO)_3(THF)]PF_6$ in dichloromethane yields comparable results, but in this case the reaction was left 18 h at room temperature.

*(N″-(2,2′-Bipyridinetricarbonylrhenium(I))-N,N′-diphenylisonicotinamidinate)tris(N,N′-diphenylisonicotinamidinate)-dirhodium(II,II) Hexafluorophosphate, **1**.* Quantities of starting product: **5**, 0.354 g (0.273 mmol); $[Re(bpy)(CO)_3(NCCH_3)]PF_6$, 0.470 g (0.767 mmol). Yield: 23% (0.118 g, 0.0632 mmol). ^1H NMR (700 MHz, CD_3CN): δ 9.04 (ddd, J = 5.5, 1.4, 0.8 Hz, 1H, Hw), 8.99 (ddd, J = 5.3, 1.4, 0.8 Hz, 1H: Hw′), 8.32 (d, J = 8.0 Hz, 1H: Hv), 8.28 (ddd, J = 8.0, 7.5, 1.5 Hz, 1H: Hy), 8.25 (d, J = 7.5 Hz, 1H: Hv′), 8.23 (ddd, J = 8.2, 7.5, 1.5 Hz, 1H: Hy′), 8.04−8.00 (m, 6H: Ha′), 7.73 (ddd, J = 7.5, 5.5, 1.5 Hz, 1H: Hx), 7.67 (d, J = 6.8 Hz, 2H: Ha), 7.64 (ddd, J = 7.5, 5.5, 1.5 Hz, 1H: Hx′), 6.99 (br, 8H: He, He′), 6.96−6.82 (m, 22H: Hd′, Hf), 6.81−6.79 (m, J = 5.3 Hz, 4H: Hd), 6.76 (dd, J = 10, 5.5 Hz, 4H: *cis* Hb′), 6.68 (d, J = 4.8 Hz, 2H: *trans* Hb′), 6.59 (d, J = 6.7 Hz, 2H: Hb), 6.52 (br, 2H: Hc), 5.91 (br, 6H: Hf′), 5.76 (br, 2H: Hf). $^{13}C\{^1H\}$ NMR (176 MHz, CD_3CN): δ 196.5; 192.5; 170.8; 170.6; 167.9; 156.1; 156.0; 154.7; 154.5; 152.4; 152.3; 151.7; 151.5; 149.68; 149.66; 149.63; 149.61; 149.5; 148.5; 144.5; 144.4; 142.2; 142.0; 129.9; 129.8; 129.7; 129.4; 128.9; 128.6; 126.57; 126.52; 125.34; 125.32; 124.7; 124.3; 124.1. HRMS (ESI, CH_3CN) (m/z): $[M - PF_6]^+$ ($C_{85}H_{64}N_{14}O_3ReRh_2$) calcd 1721.2948; found 1721.2961. IR (ATR, cm^{-1}): ν_{CO} 2032s, 1930sh, 1915s; ν_{PF} 838s. Anal. Calcd for $C_{85}H_{64}F_6N_{14}O_3PReRh_2$+DMSO: C, 5374; H, 3.63; N, 10.08; S, 1.65. Found: C, 53.56; H, 3.15; N, 9.94; S, 1.38.

*Bis(N″-(2,2′-bipyridinetricarbonylrhenium(I))-N,N′-diphenylisonicotinamidinate)bis(N,N′-diphenylisonicotinamidinate)-dirhodium(II,II) Bis(hexafluorophosphate), **2**.* Quantities of starting product: **5**, 0.354 g (0.273 mmol); $[Re(bpy)(CO)_3(NCCH_3)]PF_6$, 0.470 g (0.767 mmol). Yield: 13% (0.0859 g, 0.0352 mmol). ^1H NMR (700 MHz, CD_3CN): δ 9.27 (d, J = 4.5 Hz, 2H: Hw), 9.17 (d, J = 4.0 Hz, 2H: Hw′), 8.70−8.58 (m, 4H: Hz, Hv′), 8.50−8.35 (m, 4H: Hy, Hy′), 8.11−7.99 (m, 8H: Ha, Ha′), 7.98−7.86 (m, 2H: Hx), 7.79 (t, J = 6.0 Hz, 2H: Hx′), 7.08−6.81 (m, 24H: Hd, Hd′, He, He′), 6.79−6.71 (m, 2H: Hb′), 6.71−6.65 (m, 2H: Hb), 6.62−6.13 (br, 8H: Hc), 6.13−5.44 (br, 8H: He). $^{13}C\{^1H\}$ NMR (176 MHz, CD_3CN): δ 196.48; 196.46; 192.5; 156.11; 156.09; 156.03; 156.02; 154.7; 154.5; 151.76; 151.72; 151.70; 149.52; 149.47; 149.42; 149.41; 149.37; 149.28; 142.17; 142.14; 142.00; 141.98; 129.7; 129.40; 129.38; 128.7; 125.34; 125.32; 124.8; 124.5. HRMS (ESI, CH_3CN) (m/z): $[M - PF_6]^+$ ($C_{98}H_{72}F_6N_{16}O_6PRe_2Rh_2$) calcd 2293.2682; found 2293.2577. IR (ATR, cm^{-1}): ν_{CO} 2031s, 1930sh, 1910s; ν_{PF} 834s. Anal. Calcd for $C_{98}H_{72}F_{12}N_{16}O_6P_2Re_2Rh_2$: C, 48.28; H, 2.98; N, 9.19. Found: C, 48.10; H, 2.99; N, 9.16.

*Tris(N″-(2,2′-bipyridinetricarbonylrhenium(I))-N,N′-diphenylisonicotinamidinate)(N,N′-diphenylisonicotinamidinate)dirhodium-(II,II) Tris(hexafluorophosphate), **3**.* Quantities of starting product: **5**, 0.100 g (0.072 mmol); $[Re(bpy)(CO)_3(THF)]PF_6$, 0.154 g (0.239 mmol). Yield: 27% (0.062 g, 0.021 mmol). ^1H NMR (700 MHz, CD_3CN): δ 9.04 (dd, J = 6.0, 1.5 Hz, 1H: *trans* Hw), 9.02 (dd, J = 5.5, 1.0 Hz, 2H: *cis* Hw), 9.00−8.98 (m, 1H: *trans* Hw′), 8.98 (dd, J = 5.5,

dx.doi.org/10.1021/ic4024585 | *Inorg. Chem.* 2014, 53, 624−636

1.5 Hz, 2H: *cis* Hw′), 8.42 (d, J = 8.0 Hz, 1H: *trans* Hv), 8.37 (d, J = 8.0 Hz, 2H: *cis* Hv), 8.35 (d, J = 8.0 Hz, 1H: *trans* Hv′), 8.31−8.29 (m, 3H: *cis* Hv′, *trans* Hy), 8.28 (td, J = 8.0, 1.5 Hz, 2H: *cis* Hy), 8.24 (td, J = 8.0, 1.5 Hz, 1H: *trans* Hy′), 8.22 (td, J = 8.0, 1.5 Hz, 2H: *cis* Hy′), 8.01 (br, 2H: Ha′), 7.74 (ddd, J = 7.5, 5.5, 1.0 Hz, 1H: *trans* Hx), 7.76 (ddd, J = 7.5, 5.5, 1.0 Hz, 1H: *cis* Hx), 7.66 (td, J = 5.5, 1.0 Hz, 1H: *trans* Hx′), 7.65−7.64 (m, 4H: *cis* Hx′, *trans* Ha), 7.63 (d, J = 6.4 Hz, 4H: *cis* Ha), 6.93−6.91 (m, 6H: Hd′, *trans* He), 6.89−6.85 (m, 6H: *cis* He, He′), 6.83 (t, J = 7.0 Hv 4H: *trans* Hd), 6.80−6.77 (m, 8H: *cis* Hd), 6.63−6.58 (br, 2H: Hb′), 6.52 (d, J = 6.0 Hz, 2H: *trans* Hb), 6.51−6.45 (br, 2H: Hc′), 6.44 (t, J = 6.2 Hz, 4H: *cis* Hb), 6.39−6.30 (br, 4H: *cis* Hc), 6.30−6.22 (br, 2H: *trans* Hc), 5.80−5.66 (br, 2H: Hf′), 5.65−6.55 (br, 6H: Hf). Note: *trans* refers to the rhenium complex *trans* to the free pyridyl, and *cis* refers to the rhenium complexes *cis* to the free pyridyl of the dimer. Peaks noted br are broad. $^{13}C\{^1H\}$ NMR (176 MHz, CD_3CN): δ 196.61; 196.59; 192.6; 170.7; 168.3; 168.2; 156.26; 156.22; 156.15; 156.13; 156.78; 154.75; 154.6; 151.97; 151.90; 151.8; 151.2; 151.1; 149.5; 148.3; 144.5; 142.3; 142.19; 142.12; 141.0; 133.9; 129.8; 129.64; 129.62; 129.56; 129.53; 129.4; 129.3; 128.9; 128.8; 128.6; 126.7; 125.62; 125.56; 125.52; 125.0; 124.9; 124.5. HRMS (ESI, CH_3CN) (m/z): $[M - PF_6]^{+2}$ ($C_{111}H_{80}F_6N_{18}O_9PRe_3Rh_2$) calcd 1360.1384; found 1360.1380. IR (ATR, cm^{-1}): ν_{CO} 2030s, 1930sh, 1905s; ν_{PF} 833s. Anal. Calcd for $C_{111}H_{80}F_{18}N_{18}O_9P_3Re_3Rh_2$: C, 44.30; H, 2.68; N, 8.38. Found: C, 44.35; H, 2.78; N, 8.38.

Tetrakis((N″-(2,2′-bipyridinetricarbonylrhenium(I))-N,N′-diphenylisonicotinamidinate)dirhodium(II,II) Tetrakis-(hexafluorophosphate), ***4****.* Quantities of starting product: **5**, 0.312 g (0.241 mmol); $[Re(bpy)(CO)_3(THF)]PF_6$, 1.376 g (2.247 mmol). Yield: 50%. ^1H NMR (700 MHz, CD_3CN): δ 9.05 (ddd, J = 5.5, 1.5, 1.0 Hz, 4H: Hw), 9.01 (ddd, J = 5.0, 1.5, 1.0 Hz, 4H: Hw′), 8.34 (ddd, J = 8.0, 1.0, 0.5 Hz, 4H: Hv), 8.31 (ddd, J = 8.0, 7.0, 1.50 Hz, 4H: Hy), 8.27 (ddd, J = 8.0, 1.5, 0.5 Hz, 4H: Hv′), 8.25 (ddd, J = 8.0, 7.0, 1.50 Hz, 4H: Hy′) 7.79 (ddd, J = 7.0, 5.5, 1.5 Hz, 4H: Hx), 7.68 (ddd, J = 7.0, 5.5, 1.5 Hz, 4H: Hx′), 7.65 (d, J = 7.0 Hz, 8H: Ha), 6.91 (t, J = 7.5 Hz, 8H: He), 6.78 (t, J = 7.5 Hz, 16H: Hd), 6.43 (d, J = 7.0 Hz, 8H: Hb), 5.65−5.47 (br, 8H: Hc), 6.31−6.14 (m, 8H: Hf). $^{13}C\{^1H\}$ NMR (176 MHz, CD_3CN): δ 196.41; 196.37; 192.4; 168.2; 156.1; 155.9; 154.6; 154.5; 151.7; 150.8; 147.9; 141.9; 129.6; 129.4; 129.1; 128.90; 128.85; 128.68; 128.5; 125.3; 125.2; 124.9. HRMS (ESI, CH_3CN) (m/z): $[M - 2(PF_6)]^{+2}$ ($C_{124}H_{88}F_{12}N_{20}O_{12}P_2Re_4Rh_2$) calcd 1646.1252; found 1646.1201. IR (ATR, cm^{-1}): ν_{CO} 2032s, 1930sh, 1908s; ν_{PF} 829s. Anal. Calcd for $C_{124}H_{88}F_{24}N_{20}O_{12}P_4Re_4Rh_2$: C, 41.59; H, 2.48; N, 7.82. Found: C, 41.23; H, 2.41; N, 7.60.

Tetrakis(N,N′-diphenylisonicotinamidinate)dirhodium(II,II), ***5****.* ^1H NMR (400 MHz, CD_3CN): δ 8.01 (d, J = 3 Hz, 8H: Ha′), 7.07 (s, 16H: Hd′), 6.87 (s, 8He′), 6.83 (d, J = 3 Hz, 8H: Hb′), 6.72 (s, 8H: Hc′), 5.89 (s, 8H: Hf′) $^{13}C\{^1H\}$ NMR (176 MHz, DMSO-d_6): δ 168.0; 149.7; 149.1; 142.0; 128.8; 127.6(br); 126.6(br); 125.2; 123.8. HRMS (ESI, CH_3CN) (m/z): $[M + H]^+$ ($C_{72}H_{57}N_{12}Rh_2$) calcd 1295.2934; found 1295.2876.

Crystal Structure Determination. X-ray crystallographic data were collected from a single-crystal sample, which was mounted on a loop fiber. Data were collected with a Bruker Microstar diffractometer equipped with a Platinum 135 CCD detector at 150(2) K. The data were integrated with APEX2 software and corrected for absorption using the SADABS package.[20] Following analytical absorption corrections and solution by direct methods, the structures were refined against F^2 with full-matrix least-squares using the program SHELXL-97.[21] All H atoms were added at calculated positions and refined by use of riding models with isotropic displacement parameters based on those of the parent atoms. Anisotropic displacement parameters were employed throughout for the non-hydrogen atoms. Images were generated using Ortep III and POV-Ray.[22] X-ray quality crystals of **1** were obtained by vapor diffusion of isopropyl ether into an acetonitrile solution containing the complex.

Crystal data for **1**, $[C_{87}H_{67}N_{15}O_3ReRh_2][F_6P]\cdot 2.5(C_2H_3N)$, were collected on a Bruker Microstar at 150(2) K using Cu Kα radiation (λ = 1.54178 Å). Full-matrix, least-squares refinements on F^2 using all data; 15 021 unique reflections, M = 2010.18, triclinic, space group $P\bar{1}$, a = 12.692(2) Å, b = 17.182(3) Å, c = 21.751(3) Å, α = 75.315(8)°, β = 77.197(8)°, γ = 73.324(7)°, V = 4338.5(12) Å^3, Z = 2, R_1 [$I > 2\sigma(I)$] = 0.0605, wR_2 (all data) = 0.1422. Figures S1 and S2 display the asymmetric unit.

Computational Methods. All calculations were performed with Gaussian 03 and 09 software (G03 and G09).[23] G09 was used mainly for gas-phase optimization and vibrational frequency determinations of the bigger systems and gave identical result to G03. All TD-DFT was done on G03, G09 gave similar result, but G03 was kept for a better uniformity in the comparison with older calculated data. The initial model used before optimization comes from the solid-state structure, without any anion or solvent adducts. Optimization and IR frequency determination were carried out with the DFT method using the B3LYP functional[24] in the gas phase with the 6-31G** basis set for C, H, N, and O atoms and the relativistic LANL2DZ with effective core potentials and one additional f-type polarization function for Rh and Re atoms (α_f(Rh) = 1.350; α_f(Re) = 0.890).[25] All structures optimized successfully and had no imaginary frequencies, except **5+MeCN**. **5+MeCN** did not converge with tight conditions, and its lowest energy model still possessed a negative frequency centered on the axial rotation of the methyl group around the C−C axis of MeCN; this has minimal impact on the global properties of the dimer and was used as is. The absorption spectra and solution-state molecular orbital (MO) energies were calculated by TD-DFT, using the same method associated with the polarized continuum model (CPCM)[26] and a smaller basis set: Rh, Re, N bond to metal, the amidinate C, and the carbonyls remained unchanged, while all other remaining atoms (C, H, N) used 3-21G. Gaussview 3.09 was used to visualize MOs with an isodensity of 0.02; GaussSum 2.2 was employed to extract the absorption energies, oscillator strengths, and molecular orbital energies; and Chemissian program was used to sketch energies of MOs with their color-coded atomic orbital (AO) contributions, using 0.01 eV as the threshold for degeneracy for the MO.[27] A model of complex **8** has already been studied in our group using the same methods and was used for comparison.[10c]

RESULTS AND DISCUSSION

The synthesis of the rhenium assemblies was straightforward, and specific assemblies were prepared by varying the ratio of rhenium complex to rhodium dimer. Separation of the rhenium species was not possible by traditional silica gel chromatography, which leads to dissociation of the assemblies, whereas size-exclusion chromatography permitted product separation with no observable Re(I) dissociation. The complexes proved stable in the solid state and in most solvents, but dimethylsulfoxide and acetone displayed slow dissociation of the rhenium chromophores after a few days. Note that in the case of **2** it was not possible to separate the two possible *cis* and *trans* isomers, and they were analyzed as a mixture (see Chart S1 for a full scheme of these species).

X-ray Structural Investigation and Calculated Geometry. The structural characteristics of the assemblies have been reported for **4** and **5**.[6b] These dimers crystallize easily, presumably due to the high symmetry of the molecules. In the case of **4**, disorder from cocrystallized solvent and the hexafluorophosphate anions was observed. Both complexes **1** and **3** crystallized, but only **1** furnished X-ray quality crystals. In the case of **2**, no crystallization occurs in the same conditions used for the other complexes, possibly due to the presence of both *cis* and *trans* isomers in solution. Both complex **1** and **4** crystallized with an acetonitrile adduct in the axial position of the rhodium dimer (see Chart 1), while **5** is adduct free. Figure 1 illustrates the three dimers of the family, and a first general observation can be made: all these dimers are chiral in the solid state, due to the presence of a helicity in the amidinate phenyl

dx.doi.org/10.1021/ic4024585 | Inorg. Chem. 2014, 53, 624−636

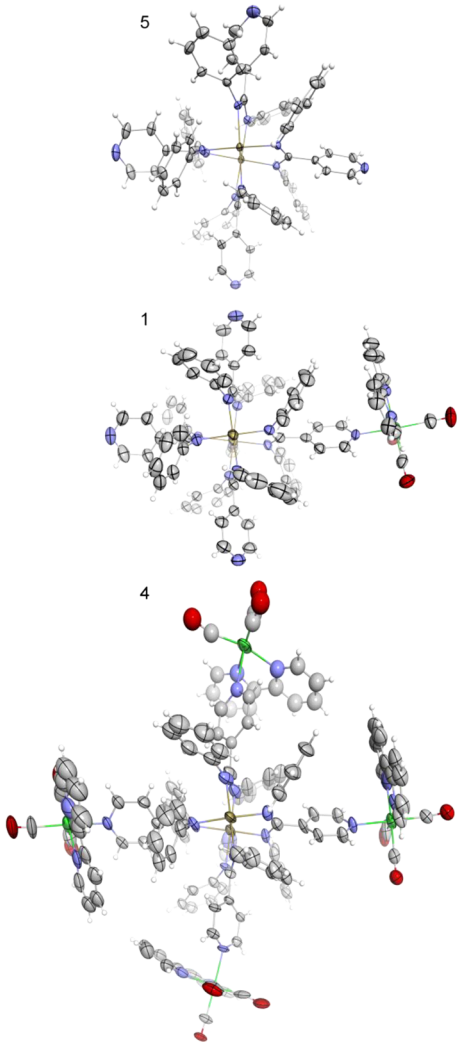

Figure 1. ORTEP view of the X-ray crystal structures of **5** (top), **1+MeCN** (center), and **4+MeCN** (bottom) (50% probability displacement ellipsoids; anion, solvent, and any other chemically equivalent molecule removed for the sake of clarity).

rings and that the racemic mixture of the two forms is found for all of the structures.

Complexes **5**, **5+MeCN**, **1**, and **4** had their geometry optimized from the crystallographic data (the latter two were modeled as charged species without anions). The computational modeling of these complexes, especially **4**, with its four attached rhenium and a total of 250 atoms, proved quite challenging, and they represent the first fully modeled structures of this class of rhodium amidinate dimers with the exception of the much smaller tetraethanimidamidate rhodium dimer.[28] Past calculations done for larger *N,N′*-arylamidinate dimers were all based on a minimalist formamidinate core model composed of 26 atoms, $[Rh_2(N_2H_2CH)_4]$; as such, they offered very little insight on functionalization effects of the amidinate.[5c,h,i,29] Due to the significant computational cost implied in modeling rhenium chromophores attached to the dimer, complexes **2** and **3** were not analyzed, as very limited knowledge would have been gained, since all their measured properties follow the trend between **1** and **4**. Complete modeling of the acetonitrile adducts of **1** and **4** was not attempted for the same reason and due to the optimization difficulty observed for **5+MeCN**. The optimized structures of **1** and **4** are good models, but the bipyridines of the Re are much farther away from the amidinate than they are in the solid state, as can be seen in Figure 2 for the case of **4**. This deviation can

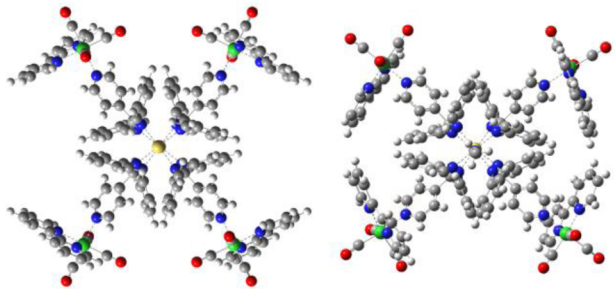

Figure 2. Optimized geometry (left) of **4** versus solid-state model **4+MeCN** (right).

be explained by the absence of dispersion modeling in our chosen method, which neglects attractive π stacking observed between the bipyridine of the rhenium and the core phenyl rings and can be a small source of discrepancy in our modeling.

The main crystallographic feature of the dimers is its Rh−Rh distances (Table 1). In our present study two elements modify it from the parent dimer **5**: the presence of an acetonitrile adduct and of the rhenium chromophores. Without the **1+MeCN** structure, our first analysis showed that **4+MeCN** and **5** have very similar Rh−Rh lengths, suggesting the acetonitrile adduct and the rhenium chromophores had little effect on the Rh−Rh bond distance. Literature examples were not conclusive in this regard: the tetradiphenylbenzamidinate (dpb) dimer (**6**), which is very similar to complex **5**, showed extensive increase in bond length when coordinated to CO, but due to the very different nature of CO and acetonitrile ligands, no conclusion could be made.[5f] The tetradiphenylformamidinate (dpf) dirhodium dimer (**7**), without any central aryl ring and thus much less steric hindrance, showed no Rh−Rh bond length increase upon axial coordination either.[5g]

The dimer **1+MeCN** crystal structure has a significantly longer (>3σ) Rh−Rh bond length when compared to both **5** and **4+MeCN**. This leads to the conclusion that an acetonitrile adduct increases the Rh−Rh bond length, whereas the addition of a Re chromophore lowers it. The first statement can be confirmed by analyzing the optimized structure of **5**: it has a Rh−Rh bond 0.03 Å shorter than the **5+MeCN** model, despite slightly elongated Rh−Rh (+0.017 Å) and Rh−N bonds (+0.044 Å) versus the X-ray data. This compares very well with the difference of 0.031 Å seen experimentally between **5** and **1+MeCN**. The effect of the Re chromophores appears to be much more subtle on the calculated models; moving from **5** to **1** reduces the Rh−Rh bond length by 0.0023 Å, while it drops by a mere 0.0014 Å when passing from **1** to **4**. The measured effect seems much higher, suggesting the computed model of **4** is not quite adequate for evaluating these bond lengths.

The acetonitrile adduct has another measurable effect on the dimer geometry: the increased length of the Rh2−N bonds (where Rh2 is binding an axial adduct). From the DFT data of **5+MeCN** we have a 0.04 Å increase in these metal−ligand bonds upon coordination of the acetonitrile. This increase is similar to **1+MeCN** (+0.04 Å) and **4+MeCN** (+0.03 Å), although it is below the 3σ error of the individual bonds for **4+MeCN**. It is clearly visible for **1+MeCN**, which has more precise bond lengths (3σ = 0.018 Å). This increase is also

dx.doi.org/10.1021/ic4024585 | *Inorg. Chem.* 2014, 53, 624−636

Table 1. Selected Parameters of the Solid-State Model and Computed DFT Models (in italics) of the Assemblies and Related Complexes

	lengths (Å)								angles (deg)	
dimer	Rh1−Rh2	Rh1−N[e]	Rh2−N[f]	Rh2−L adduct	Re−N_{py}	Re−N_{bpy}[g]	Re−C[g]	C−O[g]	N_{bpy}−Re−N_{bpy}	N−Rh−Rh−N′[g]
1 +CH_3CN	2.4365(8)	2.04(1)[g]	2.08(1)[g]	2.114(7)	2.215(5)	2.18(2)	1.93(3)	1.14(3)	75.1(3)	14.4(4)
1 (−PF_6)	*2.4211*	*2.10(1)*[h]			*2.252*	*2.198(1)*[h]	*1.930(3)*[h]	*1.158(1)*[h]	*74.45*	*14.9*
4 +CH_3CN	2.414(3)	2.06(1)[g]	2.09(3)[g]	2.17(3)	2.22(3)[g]	2.15(6)	1.90(4)	1.15(5)	76.6(15)[g]	14.6(6)
4 (−$4PF_6$)	*2.4197*	*2.105*			*2.28*	*2.200(1)*[h]	*1.930(5)*[h]	*1.158(4)*[h]	*74.5*	*14.7*
5	2.4055(8)[g]	2.054(9)[g]								12.6(4)
5	*2.4234*	*2.0976*								*14.6*
5 +CH_3CN	*2.4551*	*2.093*	*2.135*	*2.178*						*14.5*
6[a]	2.389(1)	2.05(6)								17.3
6 +CO[a]	2.435(1)	2.056(6)	2.114(6)	1.97(2)						17
7[b]	2.457(1)	2.057(1)								3.5
7 +CH_3CN[b]	2.459(1)	2.062(2)	2.066(2)	2.106(4)						16.8
8[c]					2.194(6)	2.17(1)	1.92(1)	1.15(1)	74.5(2)	
8[d] (−*triflate*)					*2.266*	*2.198(1)*[h]	*1.930(2)*[h]	*1.158(2)*[h]	*74.5*	

[a] **6**: Rh_2(*N*,*N*′-diphenylbenzamidinate)$_4$.[5f] [b] **7**: Rh_2(*N*,*N*′-diphenylformadinate)$_4$.[5g] [c] **8**: [Re(bpy)$(CO)_3$(py)] triflate.[30] [d] From the literature.[10c] [e] On the Rh without adduct. [f] On the Rh with adduct. [g] Averaged measurement; error represent the highest standard deviation between equivalent bonds and experimental error. [h] Averaged value of the calculated bonds.

observed in the case of $Rh_2(dpb)_4$ (**6**) upon coordination of CO with a 0.06 Å increase of the Rh2−N bonds, while again the formamidinate complex **7** has no significant changes. This distortion on the Rh−N distances suggests very strong steric constraints imposed on any axial adduct, stronger than the diarylformamidinate family of dimers. The rhenium chromophores do not seem to increase this steric bulk around the axial site; they actually stabilize the adduct formation due to their electron-withdrawing effect. This will be discussed later in more detail.

The rhenium−ligand bonds show no deviation in bond lengths and angles as compared to the simplest model complex, Re(bpy)$(CO)_3Py^+$ (**8**) (Table 1),[30] thus confirming that the rhenium chromophore is not subject to steric hindrance from the amidinate ligand or the other rhenium chromophores. The theoretical models of **1**, **4**, and **8** also show near identical parameters, except for the Re−N_{py} bond; in the case of **1** it is shorter by 0.014 Å versus **8**, while for **4** it is the reverse: it is 0.014 Å longer. These values make sense, as the amidinate pyridyl can be more electron rich then a free pyridyl, but the effect of the +4 charge across the dimer slightly lowers this effect. Although the crystal data reflect this trend, the bond resolution is too poor to confirm it. A survey of the Cambridge Structural Database (CSD) suggests very little changes to the Py−Re bond for functionalized pyridine derivatives, even with anionic or cationic charges attached to the pyridine, so no observable change is expected.[31]

The rhenium−rhodium assemblies can be compared to rhenium−porphyrin assemblies in the literature, both having mono- and tetrarhenium versions (although in the case of porphyrin the number of rhenium complexes was determined by the number of pyridyl units grafted to the porphyrin).[12a] The same square motif can be observed, although the porphyrin core is actually bigger, bringing the opposed rhenium chromophores 20 Å apart versus 18 Å in **4**. Like the porphyrin tetrarhenium assembly, the rhenium units are paired by two with the bipyridine ligand pointing toward each other always on the smallest side of the rectangle (14 Å by 12 Å). This arrangement seems to be due to the packing of the dimers (Figure S3); the longer side shows two intercalating T-shaped π-stacks between a bpy ring and a phenyl ring of the dimer (3.1 and 3.4 Å apart). In the case of **1** no special interaction occurs in the packing of the crystal, and no H-bonding bridges are formed by any of the three remaining pyridyl moieties.

IR Spectroscopy. All of the complexes displayed IR spectra consistent with the facial configuration of the carbonyl ligands, as indicated by the three intense CO absorptions. The peaks at 2032 cm^{-1} and the shoulder at 1930 cm^{-1} are identical for all of the species (**1** to **4**), but the last peak varies slightly, from 1915 to 1905 cm^{-1}. Although this vibration decreases with the increased number of coordinated rhenium complexes (up to three), the shift is at most marginal. The positions of these three bands are consistent with other pyridine-bound complexes, such as **8**, which has bands at 2026, 1921, and 1907 cm^{-1} (in KBr, vs ATR bulk powder measurement herein).[32] The computed frequency between **1**, **4**, and **8** gave only small differences (8 cm^{-1} max), again showing very little measurable variation (Table S1). No splitting of the IR bands of CO stretches for complexes **2** (*cis*/*trans* mix) and **3** was found, even if both these complexes have chemically different Re(I) centers. This fact, plus the similarity of all of the species, suggests that the rhenium complexes bonded to the dimer do not interact with one another: no effect is seen from steric tension or electron density brought by the other rhenium complexes. This was also observed for tetrarhenium assemblies bonded to a tetrapyridylporphyrin.[12a]

NMR Spectroscopy. The proton NMR spectra of the assemblies display a split and a broadening of the signal of the protons *ortho* to the pendant phenyl groups (only a broadening is observed for the protons in *meta* position). This effect was reported before for this type of complex and has been studied in greater detail for **5** in this work.[6a,b] The splitting of the signal is due to restricted rotation; at room temperature the phenyl rings are sterically hindered and are in a slow-exchange regime on the NMR time scale. In the crystal structure model where the rotation is totally frozen, as shown in Figure 3, the proton labeled f (in red) is oriented toward the center of an adjacent phenyl ring, creating a strong shielding effect, while proton c (in magenta) is not facing the phenyl rings. At room temperature, the rotation is slow enough to distinguish the

dx.doi.org/10.1021/ic4024585 | *Inorg. Chem.* 2014, 53, 624−636

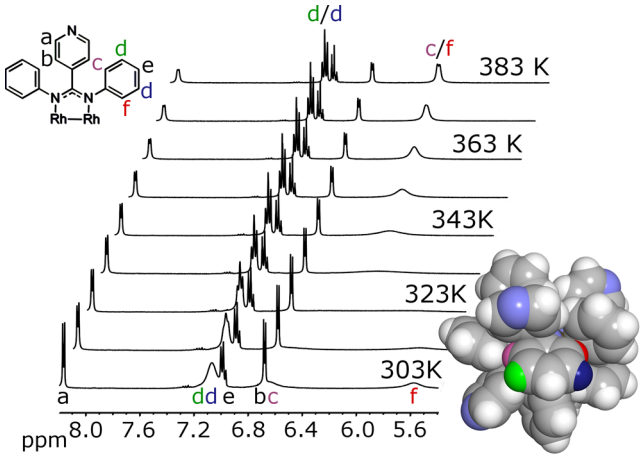

Figure 3. Variable-temperature ^{1}H NMR of **5** in d_6-DMSO. Top left: Labeling scheme of the protons. Bottom right: Space-filling model of the crystal structure of **5**, with color-coded protons.

two positions, while their ^{1}H resonances coalesce to a single signal around 325 K and form a well-defined doublet at 385 K as they can freely rotate (in DMSO, Figure 3). From the variable temperature data we can calculate a free energy of activation of 14.9 kcal/mol based on the coalescence temperature (T_C) in Kelvin and the difference in the proton splitting at that temperature ($\Delta\nu$), in Hz, using the following equation:[33] $\Delta G^* = 4.57T_C\{9.97 + \log(T_C/\Delta\nu)\}$(cal/mol). Note that these spectral features are seen in all solvents, even in acetonitrile, where one would expect a break in symmetry due to adduct formation, suggesting an exchange rate greater than the NMR time scale.

The proton chemical shifts clearly distinguish the species by the ratio of the peaks corresponding to the bipyridine ligand of the rhenium versus the peaks of the pyridyl moiety on the dimer. Upon coordination, the bpy loses its symmetry and all eight of its protons are seen as individual peaks in the rhenium assemblies due to the restricted rotation of the pyridyl ring in the presence of the phenyl rings of the amidinate. This lack of rotation of the pyridyl (either bonded or free) on the amidinate does not cause a split in its proton resonances like the phenyl rings due to a local pseudo-C_2 symmetry around the pyridine–amidinate axis (Figure 4). In the case of the rhenium-bonded pyridine, the rhenium chromophore breaks this symmetry, but it possesses a mirror plane perpendicular to the pyridine plane, thus keeping the pyridine protons as pairs. The bipyridine itself sits on one side above a phenyl ring from the dimer core, where it π-stacks and thus breaks the symmetry of the bpy proton resonances (Figure 4).

Figure 5 shows the proton NMR spectra of all the rhenium assemblies, and further splitting between the rhenium chromophores can be seen on the bpy protons in the case of **2** and **3** (around 9.00, 8.35, and 7.75 ppm). In the case of **2**, a *cis/trans* two-to-one ratio can be measured and matches the expected statistical distribution (two possibilities for the *cis* isomer vs one for the *trans* isomer). In the case of **3** the splitting is more apparent with again a two-to-one ratio of the bipyridine resonances, this time due to the chemical differences between the rhenium opposed to the free pyridyl versus the two adjacent to it. The proton signals on the dimer amidinate ligand for complexes **1** to **3** also split; however, they are poorly resolved at room temperature.

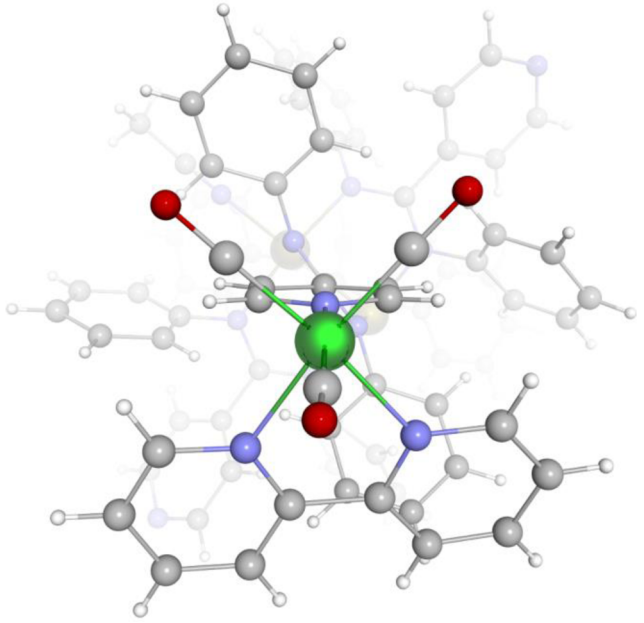

Figure 4. View of the crystal structure of **1** along the pyridine–amidinate axis.

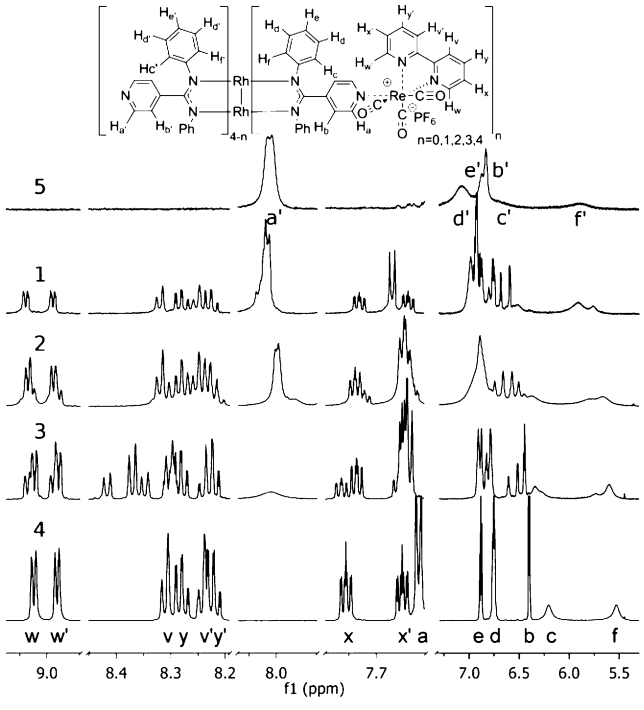

Figure 5. Proton NMR of the complexes **5**, **1**, **2**, **3**, and **4** (from top to bottom) in CD_3CN; labeling for **4** and **5** indicated as reference.

Electrochemistry. The rhodium amidinate dimers have a rich electrochemistry that is well documented. They possess three reversible or quasi-reversible metal-based single-electron redox couples, one reduction and two oxidations.[5f,g,k] The rhenium chromophores have four further redox couples (observable in MeCN), one irreversible rhenium-based oxidation, a first reversible bpy reduction, a second quasi-reversible bpy reduction, and a third irreversible reduction assumed to be centered on the rhenium. Note that in DCM only three are seen, the second bpy reduction being pushed to

dx.doi.org/10.1021/ic4024585 | Inorg. Chem. 2014, 53, 624–636

Table 2. Redox Potentials[a] of the Assemblies in Acetonitrile and Dichloromethane

		$E_{1/2}^{ox}$ (V) (ΔE (mV))			$E_{1/2}^{red}$ (V) (ΔE (mV))			
dimer	solvent	Re^{+}/Re^{2+}	Rh_2^{5+}/Rh_2^{6+}	Rh_2^{4+}/Rh_2^{5+}	$bpy^{-\bullet}/bpy$	$bpy^{2-}/bpy^{-\bullet}$	Rh_2^{3+}/Rh_2^{4+}	Re^{0}/Re^{+}
5	DCM		1.36 (180)	0.31 (100)			−1.45 (88)	
5	MeCN		1.24 (69)	0.21 (73)			−1.42 (88)	
1	MeCN	1.85	1.31 (60)	0.26 (70)	−1.18 (60)	−1.43 (120)	−1.43[b]	−1.72
2	MeCN	1.90	1.37 (130)	0.29 (87)	−1.18 (80)	−1.40 (90)	−1.51 (180)	−1.71
3	MeCN	1.86	1.38 (61)	0.36 (65)	−1.17 (63)	−1.42 (89)	−1.52 (80)	−1.73
4	MeCN	1.87	1.39 (97)	0.39 (83)	−1.17 (60)	−1.44 (89)	−1.61[c]	−1.74
4	DCM	1.86 (230)	1.43 (88)	0.43(84)	−1.12 (90)	−1.75[d]	−1.41 (120)	
6[e]	MeCN		1.08	0.05			−1.52	
6[e]	DCM		1.24	0.23			−1.58	
8[f]	MeCN	1.74			−1.09	−1.39		
8[g]	DCM	1.85			−1.2	−1.7[d]		

[a]Potentials are vs SCE; potentials without ΔE values are irreversible. [b]Superimposed with previous reduction (total two electron transfer observed). [c]Seen as a weak shoulder in square-wave experiment. [d]Corresponds to the $bpy^{2-}/bpy^{-\bullet}$ redox couple in DCM. [e]**6**: $Rh_2(dpb)_4$ from ref 5k. [f]**8**: $Re(bpy)(CO)_3(pyridine)^+$, from ref 34a. [g]**8** in DCM from ref 34b.

−1.7 V.[34] All of the redox couples for our assemblies are tabulated in Table 2.

DCM was used as a solvent only for complexes **4** and **5** to observe the effect that polarity and the coordination of acetonitrile has on the redox potentials of the assemblies versus the very similar complex **6** ($Rh_2(dpb)_4$).[5k] For **6**, it had previously been shown that the rhodium dimer's first and second oxidation potential display a 170 mV cathodic shift in acetonitrile due to its coordination and not its polarity, as DMSO and DMF actually showed an anodic shift (~100 mV) for the first oxidation. At negative potentials, the acetonitrile adduct shows only a small anodic shift (60 mV) versus the other polar solvents (200 mV). In our assemblies, both **4** and **5** showed the expected cathodic shift for the oxidation. Complex **4** shows only a 40 mV cathodic shift, much less than the 100 mV seen in **5**, and is likely due to the presence of a +4 charge already present on the assembly, making the oxidation more difficult. The reduction of **5** in DCM is at more negative potential then in MeCN, which is probably due to the interaction of **5** with MeCN being weaker than with **4** or **6**. The adduct effect is only seen during oxidation, which is stabilized by the presence of MeCN.

Looking at assemblies **1** to **5** in acetonitrile, a few trends are observable. First, the rhenium chromophores attached to the dimer do not interact with each other, showing only one wave for all the expected redox couples. The overall charge of the assembly does not affect the potential of these couples, as all have very small variations, e.g., the reversible first reduction of bpy being essentially the same for all complexes with only 10 mV variation.

On the other hand, the dirhodium redox potentials are affected by each rhenium chromophore. Both oxidations exhibit an anodic shift, the first one with a linear slope of 45 mV per rhenium, while the second oxidation follows more of an exponential curve, showing less of an effect for each added rhenium (see Figure S5). The reduction of the rhodium dimer coincides with the second bpy reduction: in **1** there is a complete superposition of the two coincidental one-electron reductions, as can be seen by square-wave (SW) voltammetry (Figure 6). The reduction of the rhodium follows a cathodic shift and is observed clearly in the SW curves of assemblies **2** and **3**. In the case of **4** the dimer reduction is almost completely masked by the four simultaneous one-electron reductions of the bipyridine on the rhenium chromophores. Only a plateau in CV

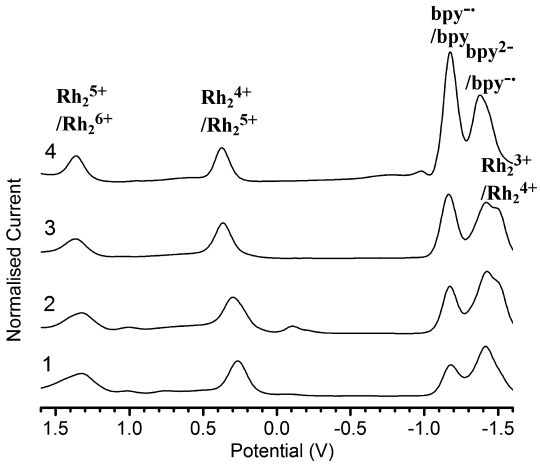

Figure 6. Square-wave voltammograms of complexes **1**, **2**, **3**, and **4** (from bottom to top) in CH_3CN. Scanning starts on the negative potential; reduction waves at −1.2 and −1.4 V are smaller due to their partial irreversibility at high negative current. Current normalized for the first oxidation maximum.

suggests the presence of the dimer reduction, re-evaluated at −1.61 V herein. At first glance, this is unexpected, since each rhenium should make the dimer less electron rich, making it easier to reduce. But at −1.4 V, the bpy in the rhenium chromophore itself undergoes its second reduction, making its total charge negative; thus the dimer actually has an increase in electron density for each rhenium chromophore present.

Calculated MO Energies. The main feature of the dimer, its metal−metal bond, is predominant in the frontier MO. The ordering of the bond interaction obtained for all of the calculated complexes is similar to previous calculations of the Rh_2 dimers.[5c,h,i] The Rh−Rh bond ordering remains the same with $\sigma^2\pi^4\delta^2\pi^{*4}\delta^{*2}$. The addition of many ligand-based or chromophore-based molecular orbitals in the upper valence region creates a further splitting of the Rh_2 δ and π bonds with strong contributions from the phenyl rings (Charts S2 to S4 illustrate selected frontier MOs). The main metal bond orbitals are labeled in Figure 7. In this figure the MO lines contain different colors to illustrate the percentile of AO of each group, red being the rhodium atoms, for example. The numerical contribution of the AO to the frontier orbitals can be found in Tables S13−S18.

dx.doi.org/10.1021/ic4024585 | Inorg. Chem. 2014, 53, 624−636

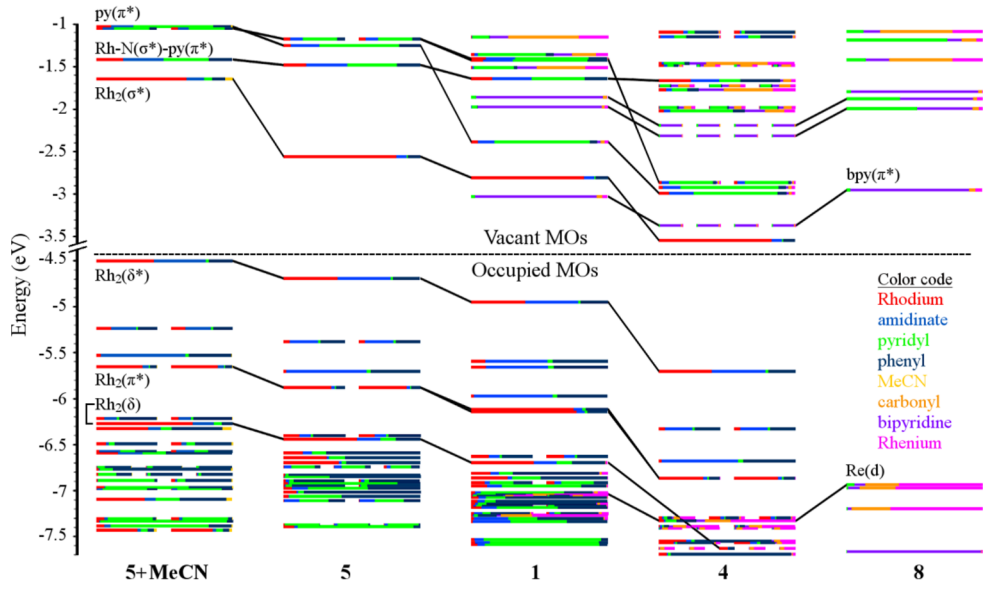

Figure 7. Frontier MO energies of modeled complexes **1**, **4**, **5**, **5+MeCN**, and **8** using a color code for the MOs indicating the percentage of AO contribution of each group found in the legend. From rb3lyp/LanL2DZ(f)[Rh,Re] 6-31G**[$NCN_{amidinate}$, $N_{py\text{-}Re}$, CO], 3-21G[C_{aryl},H, N_{py}] with CPCM (DCM or MeCN).

For all of the complexes the HOMO is the expected Rh−Rh δ^* bond, which also has some Rh−N π^* bond character. Below it, the HOMO−1 to −3 are centered on the phenyl amidinate ligand, with little metal contribution. This is followed by MOs focused on the Rh−Rh π^* bonds, here split in two sets of two degenerate orbitals (HOMO−4,−5 and −6,−7). The Rh−Rh δ bond is found mainly on HOMO−11, except for **4**. The Rh−Rh π and σ MOs are buried very deep beneath ligand-based MOs.

All of the orbitals are lowered in energy as the rhodium dimer loses core electron density by removal of the MeCN adduct or addition of the positive Re chromophore. The drop in energy among the dimers is constant for all of these orbitals, with 0.18 ± 0.03 eV from **5+MeCN** to **5**, then 0.25 ± 0.02 eV from **5** to **1**, and finally 0.70 ± 0.05 eV from **1** to **4**. This similar drop indicates that all of the occupied MOs are subject to an electrostatic effect, which is in contrast with the LUMO, the Rh−Rh σ^* bond, which drops by 0.9 eV between **5+MeCN** and **5**. This change in value is expected due to the axial coordination of the acetonitrile which directly interacts with the orbital. The Rh−Rh σ^* bond in **1** and **4** drops by the same energy as the other previously mentioned orbitals; however, the LUMO changes in **1** to the bpy π^* orbital, as expected from the electrochemical data and the MO energies of complex **8**. The MO energies of **4** should show the same change; instead it has an exaggerated lowering in energy of both its bpy π^* (LUMO +1 to +5) and Rh−Rh σ^* (LUMO) orbitals. The same effect is seen for the Re d orbitals: the first three occupied MOs in **8** show similar energy levels for **1** but are much lower in energy for **4**. The three reductions remain mostly constant for the series **1** to **4**, indicating that the model severely overestimates the effect of the +4 charge on both the rhenium- and rhodium-based MOs. A better model taking into account anions and/or adjacent solvent molecules is required.

Another issue observed in MOs of **4** is the extended delocalization of the orbitals centered on the Re chromophores, which form four closely spaced orbitals delocalized over the four rhenium sites (see Chart S3 for an example). They would be better represented as four isolated and degenerate orbitals, each on an individual rhenium site, since the first reduction observed by electrochemistry clearly indicates no communication between rhenium centers.

Photophysical Investigation and Comparison with Theoretical Models. The tetra-amidinate rhodium dimers have well-documented electronic spectra.[5f,g] In general, the amidinate dimers exhibit very small shifts in peak position in different solvents, the exception being cyano-group-containing solvents, such as acetonitrile, where its axial coordination greatly perturbs the electronic spectra of the dimers, due to the destabilization of the LUMO.

Upon titration of acetonitrile into a dichloromethane solution of **4** and **5**, their spectra change radically with the collapse of the 830 nm band, known to be the $Rh_2(\pi^*\rightarrow\sigma^*)$ transition (Figure 8). The binding constants obtained for the association of acetonitrile are 5.540(4) and 1.451(8) for **4** and **5**, respectively, which are much lower than the binding constant of 58 reported for the dpf dimer (**7**).[5g] This is expected due to increased steric bulk around the axial coordination site of the dimers. As found for **7**, only one acetonitrile forms a bond, as shown by the experimental slope value of 0.98(2) (Figure 8, insets). Interestingly, the complexation of the rhenium chromophore enhances the association constant since a more electron-deficient rhodium dimer will be further stabilized with the electron density of the acetonitrile. All the dimers studied display this solvatochromism, passing from red to green upon contact with MeCN. This is observed as well in the solid state: powders of dimers **1** to **5** display this reversible color change in the presence of acetonitrile vapor.

The spectra of the assemblies in DCM are showed in Figure 9 and indicate that only certain bands are affected by the rhenium chromophore. Their transition energies were simulated by TD-DFT, albeit with a smaller basis set to save limited computational time. Comparison of basis sets and Gaussian versions of TD-DFT calculations on **5** led to the conclusion that a better fit was obtained with the smaller basis set and G03; G09 significantly overestimated the energy of the metal-centered transitions (Tables S10, S19 to S21).

dx.doi.org/10.1021/ic4024585 | *Inorg. Chem.* 2014, 53, 624−636

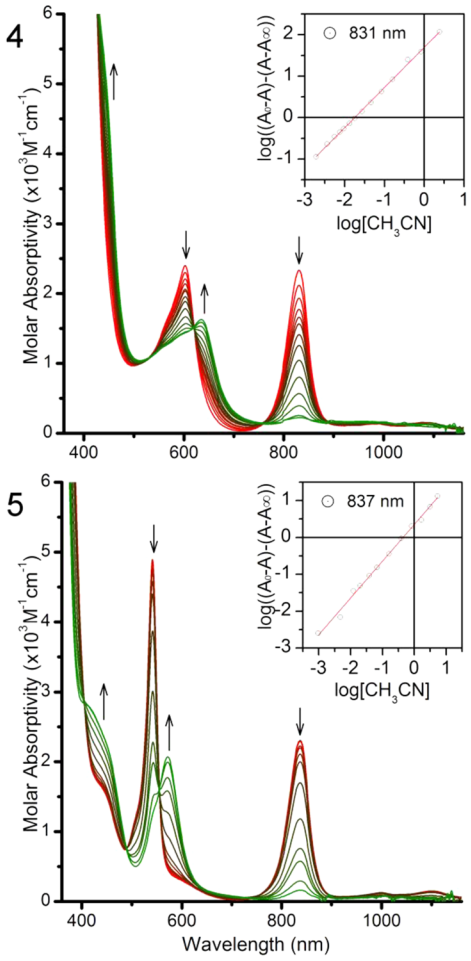

Figure 8. Changes in absorption spectra in dichloromethane of the complexes (top **4**; bottom: **5**) during titration with acetonitrile. Inset: Analysis of the spectroscopic data as a function of acetonitrile concentration.

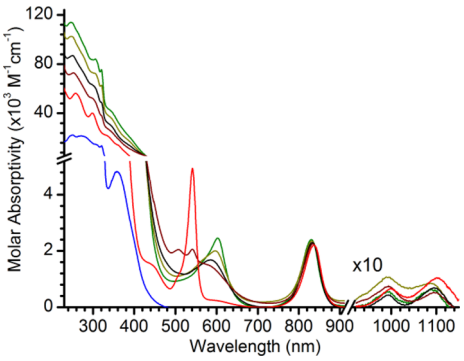

Figure 9. Absorption spectra in dichloromethane of **1** (dark red), **2** (black), **3** (dark orange), **4** (green), **5** (red), and **8** (blue); above 900 nm the signal is amplified by 10.

Complexes **5**, **1**, and **4** possess transitions of similar energies in DCM, **5+MeCN** having significantly shifted transitions (full data in Tables S8 to S12). The first transition calculated for all of the complexes is the forbidden HOMO−LUMO transition $^1Rh_2(\delta^*\rightarrow\sigma^*)$ near 1300 nm (740 nm for **5+MeCN**) with zero oscillator strength, which may be the very weak peaks near 1000 and 1100 nm (50 to 100 M^{-1} cm^{-1}). These forbidden transitions may be observed due to a vibrational loss of symmetry, and/or they could be from the forbidden triplet transition of $^3Rh_2(\pi^*\rightarrow\sigma^*)$, calculated to be at 1075 cm^{-1}. To the best of our knowledge, these transitions have never been reported previously. These NIR bands are not a trace of partly oxidized product, since upon oxidation of the dimer they do not increase; they are replaced by very broad transitions centered at 1050 and 1200 nm (see Figure S6).

The first well-known bands are the degenerate singlet $^1Rh_2(\pi^*\rightarrow\sigma^*)$ transitions calculated at 750 nm for **5**, corresponding to the peak at 838 nm. Upon coordination of the rhenium chromophores to the rhodium dimer, the peak at 838 nm is blue-shifted by about 26 cm^{-1} (approximately 2 nm) per rhenium added (Figure 9 and Table S2), showing there is only a small net increase in the energy gap between $Rh_2(\pi^*)$ and $Rh_2(\sigma^*)$ MOs. This shift is also observed in the values of the averaged $^1Rh_2(\pi^*\rightarrow\sigma^*)$ transitions of **1** and **4** (no longer degenerate due to a break in symmetry) with shifts of 48 and 105 cm^{-1}, respectively. These calculated results are closer to a previously calculated $^1Rh_2(\pi^*\rightarrow\sigma^*)$ transition centered at 986 nm for the minimalist core, but it is still significantly different. If the full basis set was employed, the result was of higher energy, at 731 nm, with G09 giving less favorable results with 706 and 711 nm for the small and big basis set (Tables S19 to S21). This result shows the limit of the method/basis set to correctly model the Rh−Rh bond, but at least the calculation gives trends of matching intensity and energy.[5c] In the case of **5+MeCN**, this transition should be blue-shifted due to the destabilization of the $^1Rh_2(\sigma^*)$ orbital. It is calculated to be at 555 nm and would fit well with the peak seen at 572 nm; however, another transition of higher intensity is also in this region.

The next two calculated transitions are more difficult to establish on the spectrum. Both are ligand-to-metal dimer charge-transfer ($^1LM_2CT$) based and are relatively weak: the first originates from a phenyl moiety and is located exactly at 650 nm for **1**, **4**, and **5**; the second is from the amidinate itself and is centered on 545 nm. The first band likely corresponds to the shoulder seen at 600 nm in the case of **5**, but in the case of **1** and **4**, this assignment is difficult due to overlapping bands.

This next transition corresponds to a Rh_2 δ^*-to-py π^* charge transfer (^{1} M_2LCT, HOMO to LUMO+1), with a relatively strong oscillator strength. In the case of **5**, the 541 nm band fits near perfectly with the calculated transition at 540 nm (0.023 o.s.). In the case of **5+MeCN**, the band calculated at 588 nm has about half the oscillator strength (0.012) and matches very well with the peak measured at 572 nm, which has half the molar absorptivity of the adduct-free dimer (Figure 10a). This corresponds to a red-shift of the ^{1} M_2LCT by 1000 cm^{-1} upon coordination of MeCN, which is similar to that of **4** (860 cm^{-1}). This is in opposition with the $^1Rh_2(\pi^*\rightarrow\sigma^*)$ band blue-shift observed and is due to the pyridine π^* MO being away from the MeCN adduct. It is less destabilized and reduces the energy gap, as can be observed in Figure 7. The addition of the Re chromophore will have the opposite effect; it will greatly reduce its energy in comparison to the Rh_2 core, thus generating another red-shift. This shift is measured at 1850 cm^{-1} (60 nm) for **4** and is calculated to be slightly higher (2330 cm^{-1}) with a transition at 619 nm (Figure 10b).

For **2** and **3** the ^{1} M_2LCT shifts less, as expected, but for **1** there are two unexpected bands seen at 541 and 507 nm, although the expected band at 572 nm is still present. This suggests that in the case of **1** the $Rh_2(\delta^*)$ → pyridyl transitions are split. This is modeled in the TD-DFT results as two distinct ^1M_2LCT transitions, one at 510 nm and the other at 625 nm.

dx.doi.org/10.1021/ic4024585 | *Inorg. Chem.* 2014, 53, 624−636

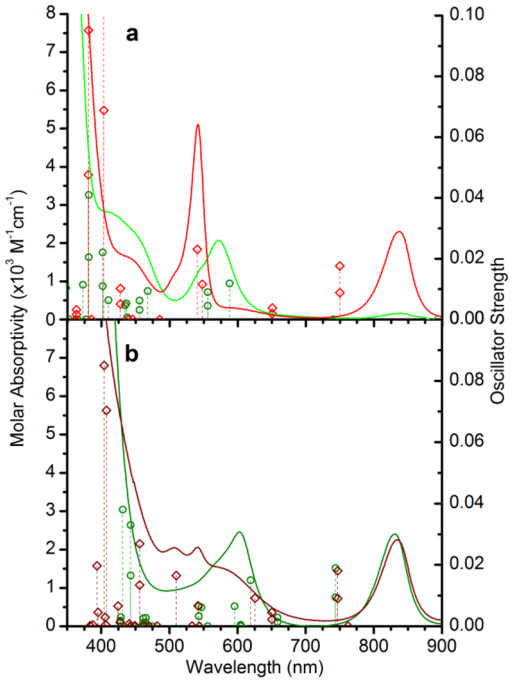

Figure 10. Absorption spectra (lines) compared to calculated TD-DFT oscillator strength (circles and diamonds); (a) **5** in DCM (red, diamonds) and acetonitrile (green, circles); (b) **1** (dark red, diamonds) and **4** (dark green, circles) both in DCM; rb3lyp/LanL2DZ(f)[Rh,Re] 6-31G**[$NCN_{amidinate}$, $N_{py\text{-}Re}$, CO], 3-21G-[C_{aryl}H, N_{py}] with CPCM (DCM or MeCN).

The remaining transition should be the previously mentioned $^1LM_2CT$, calculated to be 542 nm. We do not observe a peak at 507 nm in the case of **2** or **3**, but a definite decrease in ε is observed in that area as rhenium chromophores are added, suggesting there is still a contribution from this secondary $^1LM_2CT$.

As can be seen in Figure 9, the model rhenium chromophore **8** starts absorbing around 480 nm, but is not responsible for the sharp increase in absorption observed near 442 nm for complexes **1** to **4**. This band is due to the rhodium and should correspond to a strong amidinate to pyridine transition (^{1}LL), calculated at 443 nm for **4**, 455 nm for **1**, and 427 nm for **5**. The calculation follows the measurements, as there is an initial red-shift when the first rhenium is bonded, followed by a small blue-shift as the other rhenium chromophores are bonded.

After this transition all others become less defined, due to heavy absorption observed in the UV region. A strong second degenerate $^1Rh_2(\pi^*\rightarrow\sigma^*)$ transition was calculated, centered on HOMO−6 and −7, with stronger phenyl−amidinate character in the MOs. It is located at 403 nm (0.13 o.s. total) for **5**; however, the position of the experimental band is less obvious, and it could be a shoulder around 380 nm. In the case of **1**, this is calculated as two transitions, one at 407 nm and the other at 403 nm, which may explain the red-shift observed in that region with the addition of chromophores.

The actual contribution of the rhenium chromophore is very noticeable in the UV region, where each rhenium adds its absorbance to the total. The chromophore behaves like $Re(bpy)(CO)_3(Py)^+$ (**8**), a complex well characterized with TD-DFT studies.[10c] Model **1** evaluates these MLCT transitions at 384, 365, and 361 nm (transition 30, 40, and 42). These values are in good agreement with **8**, with its first three calculated transition being 383, 375, and 361 nm. This is a nice display of reproducibility in the TD-DFT calculation, giving similar results even after 40 transitions were calculated. For the experimental spectra, the rhenium chromophore has two distinct elements: the rhenium ^{1}MLLCT, centered at 358 nm (4800 M^{-1} cm^{-1}) for **8**, seen as a shoulder for **1** to **4** and a sharp signature bpy ^{1}IL transition band, seen for **8** at 320 nm (13500 M^{-1} cm^{-1}), readily observable in **1** to **4** at the same wavelength. It is a signature band and shows the presence of a coordinated pyridyl; for example it is fairly different from $Re(bpy)(CO)_3(MeCN)^+$, where this sharp ^{1}IL transition band is seen at 317 nm. If we plot the molar absorption versus number of chromophores at these two wavelengths, we obtain a linear fit with a slope of 4800 ± 300 and 12600 ± 200 M^{-1} cm^{-1}. If we plot the molar absorption versus number of chromophores at these two wavelengths we obtain a linear fit with a slope of 4800 ± 300 and 12600 ± 200 M^{-1} cm^{-1} for 358 and 320 nm, respectively (see Figure S4). for 358 and 320 nm, respectively (see Figure S4). These results match very well with the absorption coefficient of **8** measured at 4800 and 13500 M^{-1} cm^{-1}. At 320 nm, there is a 900 M^{-1} cm^{-1} difference, due to the absorption contribution of the pyridyl motif already present on the dimer.

The spectroelectrochemistry of **5** was also investigated in acetonitrile. At 0.35 V, two NIR bands appeared at 995 and 1280 nm (Figure 11). Similar bands have been observed for 7^+

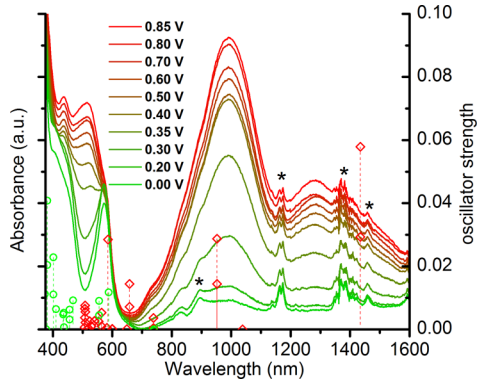

Figure 11. First oxidation of **5** in MeCN monitored by spectroscopy (applied voltage: 0.0 to 0.8 V (red to green) vs silver wire (uncorrected); electrolyte 0.1 M tBu_4NPF_6) with calculated TD-DFT oscillator strength of **5+MeCN** (green, circles) and of (**5+MeCN**)$^+$ (red, diamonds) from b3lyp/LanL2DZ(f)[Rh] 6-31G**[$NCN_{amidinate}$], 3-21G[C_{aryl}H,N] with CPCM (MeCN).*: artifacts.

at 890 and 1150 nm when the potential was held at 0.65 V.[5g] These bands are expected to be due to new transitions toward the Rh_2 δ^* MO, which is now missing an electron (see Chart S5 for calculated total electron spin density). Calculated transitions (Figure 11; vertical lines) show two main transitions in the NIR, an $^2LM_2CT$ at 1435 nm, centered on the amidinate and phenyl, and a $^2Rh_2(\pi^*\rightarrow\delta^*)$ at 952 nm. This is in agreement with the spectra, although the intensities do not match.

Emission. In terms of emission, the rhodium amidinate dimers are comparable to rhodium acetate dimers: both are known to be nonemissive, and both possess a nonradiative excited state.[5c,35] The amidinate dimers also display photochemical activity toward reduction of halogenated compounds even with near-IR radiation (λ_{irr} > 715 nm).[5c] No emission was

dx.doi.org/10.1021/ic4024585 | Inorg. Chem. 2014, 53, 624−636

observed from the attached rhenium chromophores in assemblies **1** to **4** in DCM or acetonitrile, which suggests fast quenching of the excited state of the rhenium chromophores. The rhenium complex is known to rapidly form the ^{3}MLLCT excited state after initial irradiation (<200 fs), and it should be this triplet state that is quenched by the dimer.[36] As such two possible pathways are predicted. The first path is a triplet−triplet Dexter energy transfer from the ^{3}MLLCT state of the rhenium to a nonemissive, low-energy triplet state centered on the dimer. The second pathway is a true electron transfer, leading to a transient state in the form of Rh_2(II,III) Re(I)bpy$^{-\bullet}$, before charge recombination and return to the ground state. This last path would be more similar to the observed intermolecular electron transfer outer-sphere mechanism with halogenated molecules.[5c]

These rhenium-based assemblies can be compared to ruthenium-based assemblies previously synthesized (Chart 2).[6a,13] These complexes were based on a tridentate terpyridine

Chart 2. Scheme of the Described Amidinate (Top)- and Acetate (Bottom)-Based Rh_2 Ru_4 Assemblies[4b,6a]

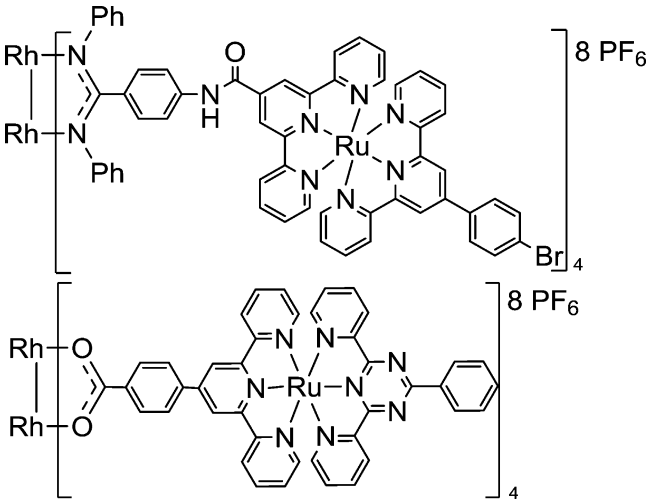

or triazine ligand bonded to the ruthenium. It was shown, in the case of the rhodium acetate assemblies, where only a phenyl spacer separates the ruthenium from the rhodium core, that energy transfer was observed for a higher energy chromophore (above 1.7 eV). Below that point, the luminescence of the chromophore was retained.[13b,c] It was shown that the nonradiative excited state of the rhodium acetate dimer was in the same range as the ^{3}MLCT of the ruthenium chromophore, thus containing insufficient driving force to quench the latter chromophores of lower energy.

An emission was still observed for amidinate-based rhodium dimers with bridged ruthenium complexes linked by an amide moiety to the dimer.[6a] The ruthenium is significantly farther away from the rhodium core than the rhenium in the present work, and this distance is enough to prohibit fast quenching of the excited state of the ruthenium chromophores. As our assemblies are much more compact with the rhenium being only a pyridyl ring away from the core of the dimer, quenching still occurs.

CONCLUSION

In the different assemblies, the rhenium chromophore base properties are not altered significantly, as demonstrated by the unchanged redox properties in electrochemistry and little change in the IR and UV−vis spectra. The rhodium dimer itself is affected, and with each rhenium chromophore added, the electron density around the dimer is lowered, making it harder to oxidize the rhodium core and giving rise to a bathochromic shift for the electronic transitions in the visible region. The presence of four chromophores also increased the binding strength of acetonitrile along the axial coordination site of the dimer, making its solvatochromism properties adjustable. Computed models were in good agreement and set a good basis for future computational modeling of rhodium dimers, thus allowing evaluation of their properties before synthesis. Although in the case of **4** the MO energies were flawed with lower energy values due to the high positive charge of the assembly, this limitation should be considered before evaluating systems using only *in silico* data.

Another interesting feature is the quenching of the rhenium emission observed in **1** to **4**. More research on the quenching of the rhenium chromophore is planned to uncover the relaxation mechanism; of particular interest will be the transient absorption spectra of the assemblies, both in the visible and in the IR.

The ability to prepare and isolate these different species permits a stepwise pathway to make larger assemblies by using the free pyridyl sites for subsequent coordination. One such application is the studies of the assemblies as chromophores for the photocatalytic production of dihydrogen using different catalysts that have an affinity for pyridine, e.g., cobalt dimethylglyoxime. Preliminary results are promising, but without a deeper understanding of the active species via theoretical models, they cannot be fully discussed at this time.

ASSOCIATED CONTENT

Supporting Information

Extra figures, tables, computational data, and data in CIF format. This material is available free of charge via the Internet at http://pubs.acs.org. X-ray crystallographic data in CIF format can also be obtained from the Cambridge Structural Database (CCDC 662536, 662537, 906876).

AUTHOR INFORMATION

Corresponding Author

*E-mail: garry.hanan@umontreal.ca. Tel: 1-514-340-5156. Fax: 1-514-343-7586.

Notes

The authors declare no competing financial interest.

ACKNOWLEDGMENTS

We are grateful to the Natural Sciences and Engineering Research Council of Canada, the Ministère de l'Éducation du Québec, and the Université de Montréal for financial support and for the Université de Montréal's Altix and Briarée supercomputers supported by le Réseau Québécois de Calculs de Haute Performances (RQCHP) and University of Manitoba's Grex supercomputer supported by Westgrid, both networks under the national supercomputing platform, Compute Canada/Calcul Canada.

REFERENCES

(1) (a) Chifotides, H. T.; Dunbar, K. R. In *Multiple Bonds between Metal Atoms*, 3rd ed.; Cotton, F. A., Murillo, C. A., Walton, R. A., Eds.; Springer: New York, 2005; p 465. (b) Cotton, F. In *Multiple Bonds between Metal Atoms*, 3rd ed.; Cotton, F. A., Murillo, C. A., Walton, R.

A., Eds.; Springer: New York, 2005; p 707. (c) Patmore, N. J. *Organomet. Chem.* **2010**, *36*, 77.
(2) (a) Korotvicka, A.; Necas, D.; Kotora, M. *Curr. Org. Chem.* **2012**, *16*, 1170. (b) Du, B. J. *Org. Process Res. Dev.* **2011**, *15*, 758. (c) Tanaka, S.; Masaoka, S.; Yamauchi, K.; Annaka, M.; Sakai, K. *Dalton Trans.* **2010**, *39*, 11218. (d) Doyle, M. P.; Duffy, R.; Ratnikov, M.; Zhou, L. *Chem. Rev.* **2010**, *110*, 704. (e) Lebel, H. In *Catalyzed Carbon-Heteroatom Bond Formation*; Wiley-VCH Verlag GmbH & Co. KGaA: 2010; p 137. (f) Doyle, M. P. *J. Org. Chem.* **2006**, *71*, 9253. (g) Timmons, D.; Doyle, M. In *Multiple Bonds between Metal Atoms*, 3rd ed.; Cotton, F. A., Murillo, C. A., Walton, R. A., Eds.; Springer: New York, 2005; p 591. (h) Lindsay, V. N. G.; Charette, A. B. *ACS Catal.* **2012**, *2*, 1221.
(3) (a) Aguirre, J. D.; Lutterman, D. A.; Angeles-Boza, A. M.; Dunbar, K. R.; Turro, C. *Inorg. Chem.* **2007**, *46*, 7494. (b) Angeles-Boza, A. M.; Bradley, P. M.; Fu, P. K. L.; Shatruk, M.; Hilfiger, M. G.; Dunbar, K. R.; Turro, C. *Inorg. Chem.* **2005**, *44*, 7262. (c) Burya, S. J.; Palmer, A. M.; Gallucci, J. C.; Turro, C. *Inorg. Chem.* **2012**, *51*, 11882. (d) Chifotides, H. T.; Lutterman, D. A.; Dunbar, K. R.; Turro, C. *Inorg. Chem.* **2011**, *50*, 12099. (e) Joyce, L. E.; Aguirre, J. D.; Angeles-Boza, A. M.; Chouai, A.; Fu, P. K. L.; Dunbar, K. R.; Turro, C. *Inorg. Chem.* **2010**, *49*, 5371. (f) Lutterman, D. A.; Fu, P. K. L.; Turro, C. *J. Am. Chem. Soc.* **2006**, *128*, 738.
(4) (a) Cooke, M. W.; Chartrand, D.; Hanan, G. S. *Coord. Chem. Rev.* **2008**, *252*, 903. (b) Cooke, M. W.; Hanan, G. S. *Chem. Soc. Rev.* **2007**, *36*, 1466. (c) Cotton, F. A.; Lin, C.; Murillo, C. A. *Acc. Chem. Res.* **2001**, *34*, 759.
(5) (a) Bear, J. L.; Van Caemelbecke, E.; Ngubane, S.; Da-Riz, V.; Kadish, K. M. *Dalton Trans.* **2011**, *40*, 2486. (b) Bear, J. L.; Han, B. C.; Li, Y. L.; Ngubane, S.; Van Caemelbecke, E.; Kadish, K. M. *Polyhedron* **2009**, *28*, 1551. (c) Lutterman, D. A.; Degtyareva, N. N.; Johnston, D. H.; Gallucci, J. C.; Eglin, J. L.; Turro, C. *Inorg. Chem.* **2005**, *44*, 5388. (d) Bear, J. L.; Han, B.; Wu, Z.; Van Caemelbecke, E.; Kadish, K. M. *Inorg. Chem.* **2001**, *40*, 2275. (e) Ren, T.; Lin, C.; Valente, E. J.; Zubkowski, J. D. *Inorg. Chim. Acta* **2000**, *297*, 283. (f) He, L. P.; Yao, C. L.; Naris, M.; Lee, J. C.; Korp, J. D.; Bear, J. L. *Inorg. Chem.* **1992**, *31*, 620. (g) Bear, J. L.; Yao, C. L.; Lifsey, R. S.; Korp, J. D.; Kadish, K. M. *Inorg. Chem.* **1991**, *30*, 336. (h) Cotton, F. A.; Feng, X. *Inorg. Chem.* **1989**, *28*, 1180. (i) Rizzi, G. A.; Casarin, M.; Tondello, E.; Piraino, P.; Granozzi, G. *Inorg. Chem.* **1987**, *26*, 3406. (j) Piraino, P.; Bruno, G.; Lo Schiavo, S.; Laschi, F.; Zanello, P. *Inorg. Chem.* **1987**, *26*, 2205. (k) Le, J. C.; Chavan, M. Y.; Chau, L. K.; Bear, J. L.; Kadish, K. M. *J. Am. Chem. Soc.* **1985**, *107*, 7195.
(6) (a) Cooke, M. W.; Santoni, M. P.; Hanan, G. S.; Proust, A.; Hasenknopf, B. *Dalton Trans.* **2009**, 3671. (b) Chartrand, D.; Hanan, G. S. *Chem. Commun.* **2008**, 727. (c) Zuo, J.-L.; Fabrizi de Biani, F.; Santos, A. M.; Kohler, K.; Kuehn, F. E. *Eur. J. Inorg. Chem.* **2003**, 449.
(7) Takeda, H.; Koike, K.; Morimoto, T.; Inumaru, H.; Ishitani, O. *Adv. Inorg. Chem.* **2011**, *63*, 137.
(8) Probst, B.; Guttentag, M.; Rodenberg, A.; Hamm, P.; Alberto, R. *Inorg. Chem.* **2011**, *50*, 3404.
(9) (a) Yui, T.; Tamaki, Y.; Sekizawa, K.; Ishitani, O. *Top. Curr. Chem.* **2011**, *303*, 151. (b) Kumar, B.; Smieja, J. M.; Sasayama, A. F.; Kubiak, C. P. *Chem. Commun.* **2012**, *48*, 272.
(10) (a) Kumar, A.; Sun, S.-S.; Lees, A. J. *Top. Organomet. Chem.* **2010**, *29*, 1. (b) Patrocinio, A. O. T.; Brennaman, M. K.; Meyer, T. J.; Murakami Iha, N. Y. *J. Phys. Chem. A* **2010**, *114*, 12129. (c) Chartrand, D.; Castro, R. C. A.; Hanan, G. S. *Inorg. Chem.* **2012**, *51*, 12738.
(11) Barber, J. *Philos. Trans. R. Soc., A* **2007**, *365*, 1007.
(12) (a) Casanova, M.; Zangrando, E.; Iengo, E.; Alessio, E.; Indelli, M. T.; Scandola, F.; Orlandi, M. *Inorg. Chem.* **2008**, *47*, 10407. (b) Slone, R. V.; Hupp, J. T. *Inorg. Chem.* **1997**, *36*, 5422. (c) Kon, H.; Tsuge, K.; Imamura, T.; Sasaki, Y.; Ishizaka, S.; Kitamura, N. *Inorg. Chem.* **2006**, *45*, 6875. (d) Splan, K. E.; Keefe, M. H.; Massari, A. M.; Walters, K. A.; Hupp, J. T. *Inorg. Chem.* **2002**, *41*, 619.
(13) (a) Cooke, M. W.; Santoni, M. P.; Hanan, G. S.; Loiseau, F.; Proust, A.; Hasenknopf, B. *Inorg. Chem.* **2008**, *47*, 6112. (b) Cooke, M. W.; Hanan, G. S.; Loiseau, F.; Campagna, S.; Watanabe, M.; Tanaka, Y. *J. Am. Chem. Soc.* **2007**, *129*, 10479. (c) Cooke, M. W.; Hanan, G. S.; Loiseau, F.; Campagna, S.; Watanabe, M.; Tanaka, Y. *Angew. Chem., Int. Ed.* **2005**, *44*, 4881.
(14) (a) Gans, P.; Sabatini, A.; Vacca, A. *Anal. Chim.* **1999**, *89*, 45. (b) Gans, P.; Sabatini, A.; Vacca, A. *Talanta* **1996**, *43*, 1739.
(15) Connelly, N.; Geiger, W. *Chem. Rev.* **1996**, *96*, 877.
(16) Schmidt, S. P.; Trogler, W. C.; Basolo, F.; Urbancic, M. A.; Shapley, J. R. In *Inorganic Syntheses*; John Wiley & Sons, Inc.: New York, 2007; p 41.
(17) Hevia, E.; Perez, J.; Riera, V.; Miguel, D.; Kassel, S.; Rheingold, A. *Inorg. Chem.* **2002**, *41*, 4673.
(18) Caspar, J. V.; Meyer, T. J. *J. Phys. Chem.* **1983**, *87*, 952.
(19) Casey, C. P.; O'Connor, J. M. *Organometallics* **1985**, *4*, 384.
(20) (a) *SAINT*, version 7.68A; Bruker AXS Inc.: Madison, WI, 2009. (b) Sheldrick, G. M. *SADABS*, version 2008/1; Bruker AXS Inc.: Madison, WI, 2008.
(21) Sheldrick, G. M. *Acta Crystallogr., Sect. A: Found. Crystallogr.* **2008**, *A64*, 112.
(22) (a) Farrugia, L. J. *J. Appl. Crystallogr.* **1997**, *30*, 565. (b) *POV-Ray*, version 3.6; Persistence of Vision Pty. Ltd.: Williamstown, Victoria, Australia, 2004.
(23) (a) Frisch, M. J.; Trucks, G. W.; Schlegel, H. B.; Scuseria, G. E.; Robb, M. A.; Cheeseman, J. R.; Montgomery, J. A., Jr.; Vreven, T.; Kudin, K. N.; Burant, J. C.; Millam, J. M.; Iyengar, S. S.; Tomasi, J.; Barone, V.; Mennucci, B.; Cossi, M.; Scalmani, G.; Rega, N.; Petersson, G. A.; Nakatsuji, H.; Hada, M.; Ehara, M.; Toyota, K.; Fukuda, R.; Hasegawa, J.; Ishida, M.; Nakajima, T.; Honda, Y.; Kitao, O.; Nakai, H.; Klene, M.; Li, X.; Knox, J. E.; Hratchian, H. P.; Cross, J. B.; Bakken, V.; Adamo, C.; Jaramillo, J.; Gomperts, R.; Stratmann, R. E.; Yazyev, O.; Austin, A. J.; Cammi, R.; Pomelli, C.; Ochterski, J. W.; Ayala, P. Y.; Morokuma, K.; Voth, G. A.; Salvador, P.; Dannenberg, J. J.; Zakrzewski, V. G.; Dapprich, S.; Daniels, A. D.; Strain, M. C.; Farkas, O.; Malick, D. K.; Rabuck, A. D.; Raghavachari, K.; Foresman, J. B.; Ortiz, J. V.; Cui, Q.; Baboul, A. G.; Clifford, S.; Cioslowski, J.; Stefanov, B. B.; Liu, G.; Liashenko, A.; Piskorz, P.; Komaromi, I.; Martin, R. L.; Fox, D. J.; Keith, T.; Al-Laham, M. A.; Peng, C. Y.; Nanayakkara, A.; Challacombe, M.; Gill, P. M. W.; Johnson, B.; Chen, W.; Wong, M. W.; Gonzalez, C.; Pople, J. A. *Gaussian 03*, Revision C.02; Gaussian, Inc.: Wallingford, CT, 2004. (b) Frisch, M. J.; Trucks, G. W.; Schlegel, H. B.; Scuseria, G. E.; Robb, M. A.; Cheeseman, J. R.; Scalmani, G.; Barone, V.; Mennucci, B.; Petersson, G. A.; Nakatsuji, H.; Caricato, M.; Li, X.; Hratchian, H. P.; Izmaylov, A. F.; Bloino, J.; Zheng, G.; Sonnenberg, J. L.; Hada, M.; Ehara, M.; Toyota, K.; Fukuda, R.; Hasegawa, J.; Ishida, M.; Nakajima, T.; Honda, Y.; Kitao, O.; Nakai, H.; Vreven, T.; Montgomery, J. A., Jr.; Peralta, J. E.; Ogliaro, F.; Bearpark, M.; Heyd, J. J.; Brothers, E.; Kudin, K. N.; Staroverov, V. N.; Kobayashi, R.; Normand, J.; Raghavachari, K.; Rendell, A.; Burant, J. C.; Iyengar, S. S.; Tomasi, J.; Cossi, M.; Rega, N.; Millam, N. J.; Klene, M.; Knox, J. E.; Cross, J. B.; Bakken, V.; Adamo, C.; Jaramillo, J.; Gomperts, R.; Stratmann, R. E.; Yazyev, O.; Austin, A. J.; Cammi, R.; Pomelli, C.; Ochterski, J. W.; Martin, R. L.; Morokuma, K.; Zakrzewski, V. G.; Voth, G. A.; Salvador, P.; Dannenberg, J. J.; Dapprich, S.; Daniels, A. D.; Farkas, Ö.; Foresman, J. B.; Ortiz, J. V.; Cioslowski, J.; Fox, D. J. *Gaussian 09*, Revision D.01; Gaussian, Inc.: Wallingford, CT, 2009.
(24) (a) Lee, C.; Yang, W.; Parr, R. G. *Phys. Rev. B: Condens. Matter* **1988**, *37*, 785. (b) Becke, A. D. *J. Chem. Phys.* **1993**, *98*, 5648.
(25) (a) Hay, P. J.; Wadt, W. R. *J. Chem. Phys.* **1985**, *82*, 299. (b) Ehlers, A. W.; Boehme, M.; Dapprich, S.; Gobbi, A.; Hoellwarth, A.; Jonas, V.; Koehler, K. F.; Stegmann, R.; Veldkamp, A.; et al. *Chem. Phys. Lett.* **1993**, *208*, 111.
(26) (a) Barone, V.; Cossi, M. *J. Phys. Chem. A* **1998**, *102*, 1995. (b) Cossi, M.; Rega, N.; Scalmani, G.; Barone, V. *J. Comput. Chem.* **2003**, *24*, 669.
(27) (a) Dennington, R., II; Keith, T.; Millam, J.; Eppinnett, K.; Hovell, W. L.; Gilliland, R. *Gaussview 3.09*; Semichem, Inc.: Shawnee Mission, KS, 2003. (b) O'Boyle, N. M.; Tenderholt, A. L.; Langner, K. M. *J. Comput. Chem.* **2008**, *29*, 839. (c) Skripnikov, L. *Chemissian*, version 3.3; 2005.

(28) Pruchnik, F. P.; Pruchnik, H.; Kochel, A. *Polyhedron* **2009**, *28*, 769.
(29) Kawamura, T.; Maeda, M.; Miyamoto, M.; Usami, H.; Imaeda, K.; Ebihara, M. *J. Am. Chem. Soc.* **1998**, *120*, 8136.
(30) Oshin, K.; Landis, A. M.; Smucker, B. W.; Eichhorn, D. M.; Rillema, D. P. *Acta Crystallogr. Sect. E: Struct. Rep. Online* **2004**, *E60*, m1126.
(31) (a) Allen, F. H. *Acta Crystallogr. B* **2002**, *58*, 380. (b) Bruno, I. J.; Cole, J. C.; Edgington, P. R.; Kessler, M.; Macrae, C. F.; McCabe, P.; Pearson, J.; Taylor, R. *Acta Crystallogr. B* **2002**, *58*, 389.
(32) Casanova, M.; Zangrando, E.; Munini, F.; Iengo, E.; Alessio, E. *Dalton Trans.* **2006**, 5033.
(33) (a) Dickson, P. M.; McGowan, M. A. D.; Yearwood, B.; Heeg, M. J.; Oliver, J. P. *J. Organomet. Chem.* **1999**, *588*, 42. (b) Sanders, J. K. M.; Hunter, B. K. *Modern NMR Spectroscopy: A Guide for Chemists*; Oxford University Press: USA, 1993. (c) Michinori, O. *Methods in Stereochemical Analysis, Vol. 4: Applications of Dynamic NMR Spectroscopy to Organic Chemistry*; VCH: New York, 1985.
(34) (a) Sacksteder, L.; Zipp, A. P.; Brown, E. A.; Streich, J.; Demas, J. N.; DeGraff, B. A. *Inorg. Chem.* **1990**, *29*, 4335. (b) Kuehn, F. E.; Zuo, J.-L.; Fabrizi de Biani, F.; Santos, A. M.; Zhang, Y.; Zhao, J.; Sandulache, A.; Herdtweck, E. *New J. Chem.* **2004**, *28*, 43.
(35) (a) Bradley, P. M.; Bursten, B. E.; Turro, C. *Inorg. Chem.* **2001**, *40*, 1376. (b) Liu, L. M.; Bear, J. L. *Acta Phys.-Chim. Sin.* **1989**, *5*, 644.
(36) Vlček, A.; Busby, M. *Coord. Chem. Rev.* **2006**, *250*, 1755.